ADVANCED FUNCTIONAL MATERIALS

Supporting Information

for *Adv. Funct. Mater.*, DOI: 10.1002/adfm.201806485

Multicore Liquid Perfluorocarbon-Loaded Multimodal Nanoparticles for Stable Ultrasound and ^{19}F MRI Applied to In Vivo Cell Tracking

*Olga Koshkina, Guillaume Lajoinie, Francesca Baldelli Bombelli, Edyta Swider, Luis J. Cruz, Paul B. White, Ralf Schweins, Yusuf Dolen, Eric A. W.van Dinther, N. Koenvan Riessen, Sarah E. Rogers, Remco Fokkink, Ilja K. Voets, Ernst R. H.van Eck, Arend Heerschap, Michel Versluis, Chris L.de Korte, Carl G. Figdor, I. Jolanda M.de Vries, and Mangala Srinivas**

Supporting Information

Multicore Liquid Perfluorocarbon-loaded Multimodal Nanoparticles for Stable Ultrasound and ^{19}F MRI Applied to In Vivo Cell Tracking

*Olga Koshkina[#], Guillaume Lajoinie[#], Francesca Baldelli Bombelli[‡], Edyta Swider[‡], Luis J. Cruz, Paul B. White, Ralf Schweins, Yusuf Dolen, Eric van Dinther, N. Koen van Riessen, Sarah E. Rogers, Remco Fokkink, Ilja K. Voets, Ernst R. H. van Eck, Arend Heerschap, Michel Versluis, Chris L. de Korte[‡], Carl Figdor[‡], I. Jolanda M. de Vries[‡], Mangala Srinivas**

Dr. O. Koshkina, E. Swider MSc, Dr. Y. Dolen, E. van Dinther, N. K. van Riessen, Prof. Dr. C. G. Figdor, Prof. Dr. I. J. M. de Vries, Dr. M. Srinivas
Department of Tumor Immunology
Radboud Institute for Molecular Life Sciences (RIMLS)
Geert Grooteplein Zuid 28, 6525 GA, Nijmegen, The Netherlands
E-mail: mangala.srinivas@radboudumc.nl

Dr. O. Koshkina
Physical Chemistry of Polymers
Max Planck Institute for Polymer Research
Ackermannweg 10, 55128 Mainz, Germany

Dr. Guillaume Lajoinie, Prof. Dr. Michel Versluis, Prof. Dr. C.L. de Korte
Physics of Fluids group
Technical Medical (TechMed) Centre and MESA+ Institute for Nanotechnology
University of Twente,

Drienerlolaan 5, 7522 NB, Enschede, The Netherlands

Prof. Dr. Francesca Baldelli Bombelli
Laboratory of Supramolecular and BioNano Materials (SupraBioNanoLab),
Department of Chemistry, Materials, and Chemical Engineering “Giulio Natta”
Politecnico di Milano
Via Luigi Mancinelli 7, 20131 Milan, Italy

Dr. L.J. Cruz
Translational Nanobiomaterials and Imaging, Department of Radiology
Leiden University Medical Centre
Albinusdreef 2, 2333 ZA, Leiden, The Netherlands

Dr. P.B. White, Dr. E. R. H. van Eck
Institute for Molecules and Materials, Radboud University
Heyendaalseweg 135, 6525 AJ, Nijmegen, The Netherlands

Dr. R. Schweins
Institut Laue – Langevin, DS / LSS
71 Avenue des Martyrs, Grenoble

Dr. S.E. Rogers
ISIS Pulsed Neutron and Muon Source, Science and Technology Facilities Council, Rutherford Appleton Laboratory, Harwell Oxford, United Kingdom

R. Fokkink, Ing.
Department of Agrotechnology and Food Sciences, Physical Chemistry and Soft Matter, Wageningen University, 6708 WE, Wageningen, Netherlands

Prof. Dr. I. K. Voets
Laboratory of Self-Organizating Soft Matter, Laboratory of Macromolecular and Organic Chemistry
Department of Chemical Engineering and Chemistry & Institute for Complex Molecular Systems, Eindhoven University of Technology
De Rondom 70, 5612 AP, Eindhoven, The Netherlands

Prof. Dr. Arend Heerschap, Prof. Dr. Chris L. de Korte
Department of Radiology and Nuclear Medicine, Radboudumc
Geert Grooteplein Zuid 10, 6525 GA Nijmegen, The Netherlands

[#]Authors contributed equally

[‡]Authors contributed equally

[*]Corresponding author: mangala.srinivas@radboudumc.nl

Contents

1 Characterization of Nanoparticles

1.1 Additional Characterization of nanoparticles used for attenuation measurements

Table S1. Additional characterization of nanoparticles used for attenuation measurements with quantitative ^{19}F NMR spectroscopy (376 MHz, D_2O) to determine the PFCE content and multi-angle dynamic light scattering (θ = 30°-150°).

Sample	PFC content (wt.-%)	R_h / nm	μ_2 (90°)
PFCE NP 1 (with gadoteridol)	17	129	0.16
PFCE NP 2 (with gadoteridol)	32	119	0.08
PFCE NP 3	37	149	0.2
PFCE NP 4	36	141	0.09
PFOB NP 1 (with gadoteridol)	29	116	0.14
PFOB NP 2	23	118	0.2
PFOB NP 3	29	97	0.14
PFOB NP 4 (with gadoteridol)	27	109	0.11

1.2 Additional SANS data and further characterization of nanoparticles used for SANS

Table S2. Coherent neutron scattering length densities (SLD) of nanoparticle components

Compound	Molecular Formula	Bulk density (g/cm-3)	SLD ($Å^{-2}$)
PLGA[1]	$C_5H_6O_4$	1.34	2.11×10^{-6}
PFCE[2]	$C_{10}F_{20}O$	1.78	3.87×10^{-6}
heavy water	D_2O	1.1	6.36×10^{-6}
light water	H_2O	1.0	-0.59×10^{-6}
H_2O/D_2O (36/64 *v:v*)	x_{H2O} = volume fraction of H_2O $SLD_{solvent} = x_{H2O}\times SLD_{H2O}+(1-x_{H2O})\times SLD_{D2O}$		3.87×10^{-6}
H_2O/D_2O (61/39 *v:v*)			2.11×10^{-6}

Table S3. Characterization of nanoparticles used in SANS measurements on figure 4 (main manuscript and figure S4 (SI) with multi-angle dynamic and static light scattering and NMR.

Sample	PFCE-content (NMR) wt.-%	R_h / nm	μ_2 (90°)	R_g / nm (SLS)
PFCE-particles (with gadoteridol)	40	158	0.06	130
PFCE-capsules	13	67	0.12	55
non-loaded PLGA particles	0	121	0.01	112

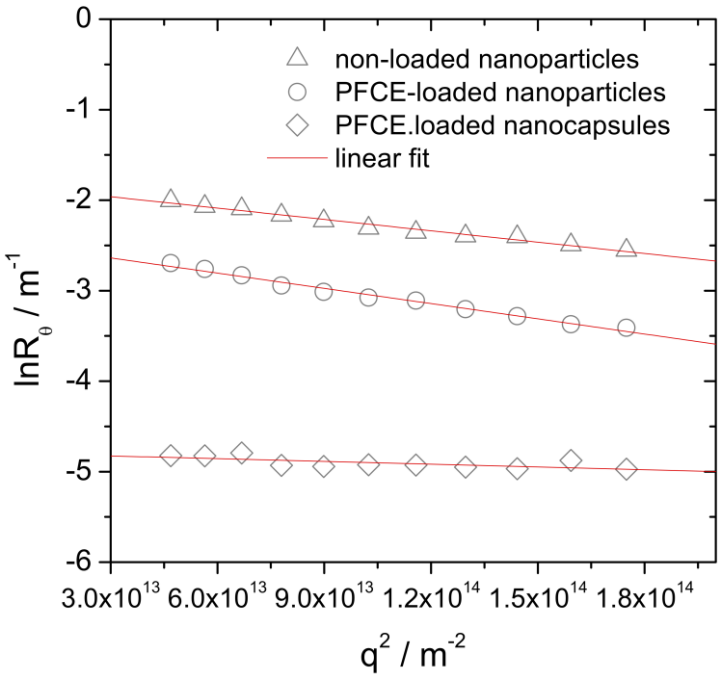

Figure S1. Guinier analysis of static light scattering to determine radius of gyration, R_g.

Table S4. Results of fitting the scattering patterns of **nanocapsules** with a core-shell model.

	D_2O	**H_2O/D_2O 36/64**	**H_2O/D_2O 61/39**
vol. fraction (fixed)	0.007	0.007	0.007
radius [nm] (linked)	19±0.07	19	19
thickness [nm] (linked)	18±0.09	18	18
SLD core [Å^{-2}] (fixed)	3.87e-6	3.87e-6	3.87e-6
SLD shell [Å^{-2}]	2.78e-6	2.35e-6	2.12e-6
SLD solvent [Å^{-2}] (fixed)	6.36e-6	3.87e-6	2.11e-6
Distribution of radius	0.5	0.4	0.3
Distribution of thickness	0.4	0.5	0.9
background	0.0055	0.012	0.050
Chi2/Npts	7.2	5.0	2.4

Table S5. Results of fitting the scattering patterns of PFCE-loaded **nanoparticles** with fractal core-shell model in D_2O and H_2O/D_2O 36/46 mixture using simultaneous fitting and single fit in H_2O/D_2O 61/39 mixture with a fractal sphere model.

	D_2O	**H_2O/D_2O 36/64**	**H_2O/D_2O 61/39**
vol. fraction	0.007	0.007	0.016
block radius [nm]	12	12	11
shell thickness [nm]	4	4	-
corr. length ξ [nm]	38	38	68
fractal dimension	3.2	3.2	2.7
SLD core [Å^{-2}]	5.64e-6	3.59e-6	2.88e-6
SLD shell [Å^{-2}]	3.26e-6	2.54e-6	-
SLD solvent [Å^{-2}]	6.36e-6	3.87e-6	2.11e-6
Distribution of radius	0.6	0.5	0.5
background	0.0037	0.012	0.021
Chi2/Npts	2.37		0.81

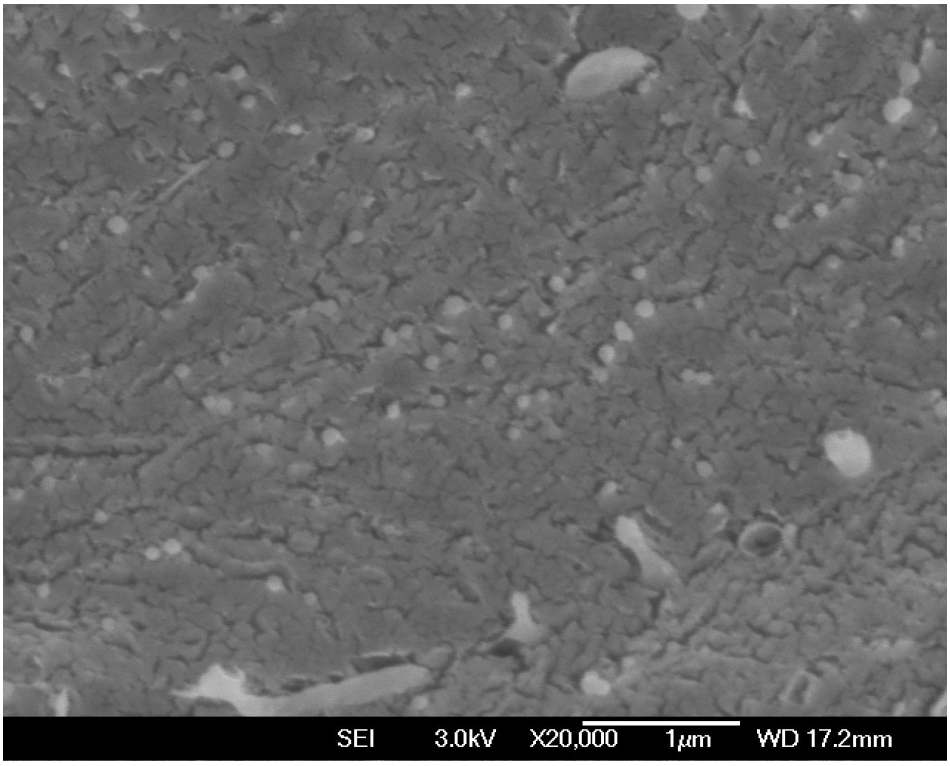

Figure S2. CryoSEM micrograph of PFCE-loaded nanocapsules. c=10 mg mL^{-1} in H_2O. Scale bar 1 μm.

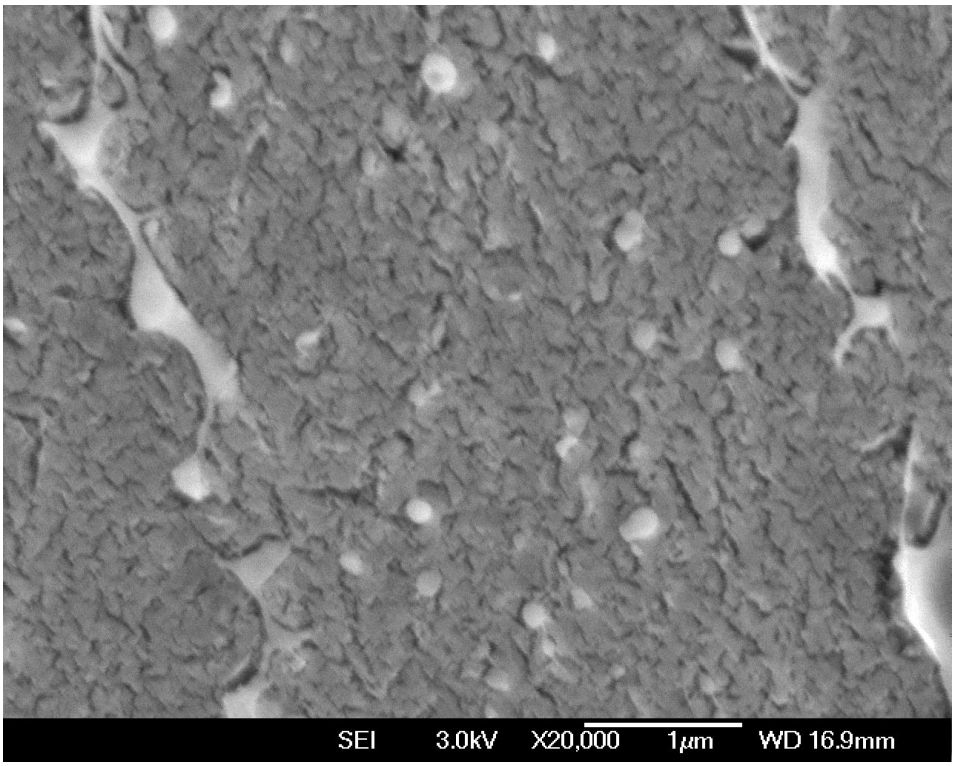

Figure S3. cryoSEM micrograph of PFCE-loaded nanoparticles. c=10 mg mL^{-1} in H_2O. Scale bar 1 μm.

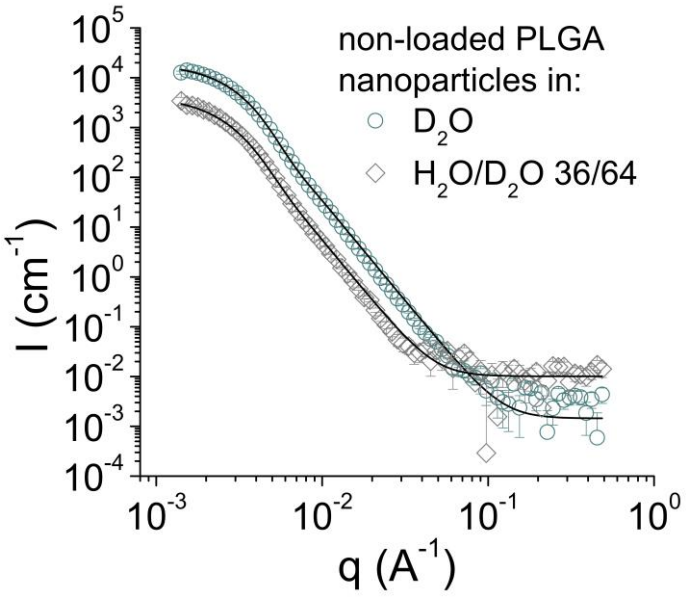

Figure S4. SANS scattering patterns of non-loaded PLGA nanoparticles. c = 10 mg mL^{-1}.

Table S6. Fit results of non-loaded PLGA nanoparticles using a sphere model with a Schulz size distribution.

	D_2O	H_2O/D_2O 36/64
vol. fraction	0.007	0.007
radius [nm] (linked)	53	53
SLD sphere [$Å^{-2}$]	2.34e-6	2.21e-6
SLD solvent (fixed)	6.36e-6	3.87e-6
polydispersity	0.3	0.4
background	0.0014	0.01
Chi2/Npts	6.24	

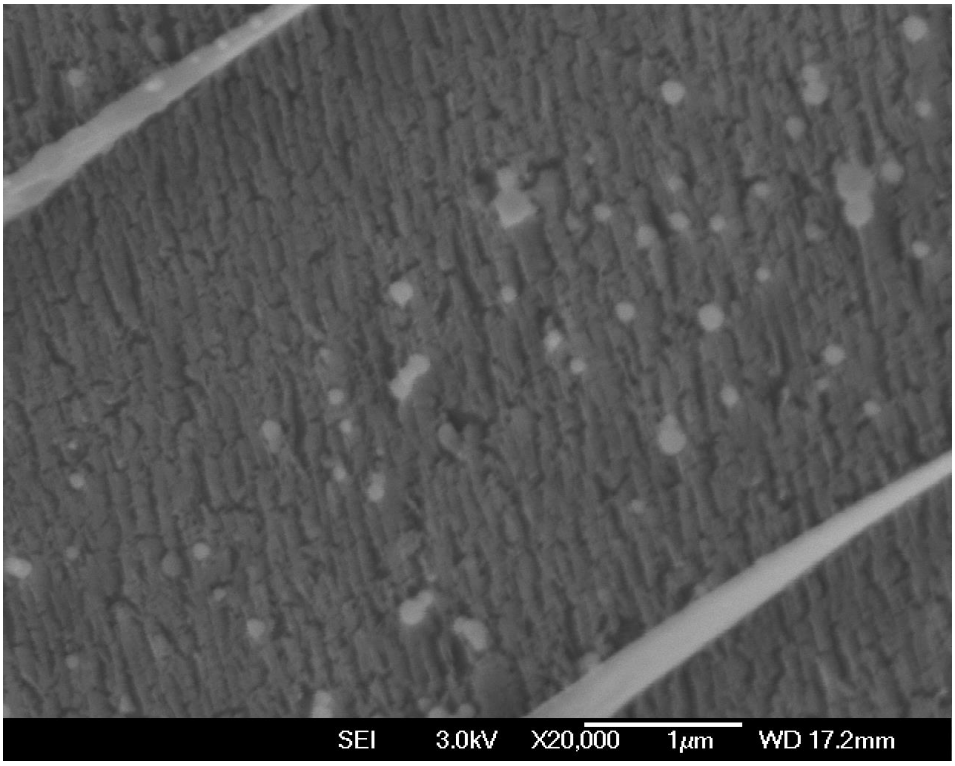

Figure S5. cryoSEM micrograph of non-loaded PLGA nanoparticles. c=10 mg mL^{-1} in H_2O. Scale bar 1 µm. The approximate radius is around 70±40 nm. Some rod-like aggregates are present in the sample.

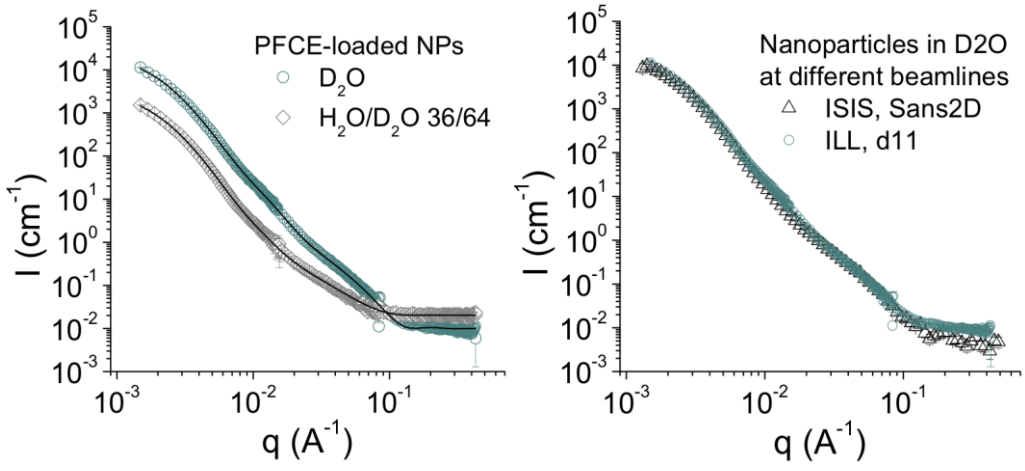

Figure S6. Left: SANS scattering patters of PFCE-loaded nanoparticles measured in D_2O and H_2O/D_2O 36/64 with fit-curves obtained with fractal core-shell model (black curves, measured at ILL. Right: comparison of SANS curves measured at ILL beamline and at ISIS beamline in D_2O. Here SANS patterns of a different batch of nanoparticles prepared without gadoteridol was used (PFCE-content 26 wt.-%)**.**

Table S7. Comparison of fitting results of PFCE-loaded nanoparticles measured at ILL with fractal core-shell model in D_2O and H_2O/D_2O 36/46 (SANS curves shown on figure S6).[i]

	ILL	
	D_2O	**H_2O/D_2O 36/64**
vol. fraction	0.007	0.007
block radius [nm]	9	9
shell thickness [nm]	4	4
corr. length ξ [nm]	48	48
fractal dimension	3.1	3.1
SLD core [$Å^{-2}$]	5.58e-6	3.86e-6
SLD shell [$Å^{-2}$]	3.27 e-6	2.45 e-6
SLD solvent [$Å^{-2}$]	6.36e-6	3.87e-6
Distribution of radius	0.6	0.6
background	0.0099	0.020
Chi2/Npts	2.53	
Further parameters		
R_g [nm] (SLS, Guinier)	129	
R_g [nm] (SANS)	121	

[i]Different sample than presented in the main text.

Supplementary Experimental Set Up

SANS D11 experimental details:

SANS measurements on D11[3] were done using 3 sample-detector distances of 1.5m, 8m and 39m, with corresponding collimation distances of 8m, 8m and 40.5m. The wavelength used was 6 Å, with a FWHM of 9%. Cylindrical Hellma cells were placed in a thermostated sample changer, the temperature was kept constant at 25 °C. A neutron beam of 13mm in diameter was employed.

Scattering intensities were recorded using a two-dimensional position-sensitive ^{3}He detector with a pixel size of 7.5 x 7.5 mm^2 and an active area of 96 x 96 cm^2. A dark current was measured and subtracted from all data. Solvents were measured and subtracted, too, taking into account the transmission values of all samples and solvents as obtained by a dedicated measurement. The data were first corrected pixel by pixel and in a second step radially regrouped in order to obtain a one-dimensional scattering curve in the form Intensity vs. Q. Data were put on an absolute scale making use of the secondary calibration standard H_2O (cross-calibrated against h/d polymer blends), which has been measured in a 1 mm Hellma cell. The differential scattering cross section for H_2O with a thickness of 1 mm has been determined to 0.983 1/cm for D11 at 6 Å neutron wavelength and 25 °C. Data were reduced[4] using ILL´s standard software package LAMP[5, 6].

Supplementary Discussion 1: Description of SANS fitting and comparison of SANS results with SLS and cryoSEM

As briefly discussed in the main manuscript, for the fitting of the form factor of core-shell nanocapsules, we used a core-shell model, with a Schulz distribution of core radius and shell thickness. We applied simultaneous fitting approach to fit all three curves, in which radius and thickness in all three solvents were linked to each other (

Table S4). The SLD of the core fixed at SLD of pure PFCE. When SLD of the core was left free, a very similar SLD value was still returned using same initial parameters. This result confirms the results of HOESY-NMR (compare Supplementary Discussion 2), which revealed that in nanocapsules PFCE is not or only minorly hydrated, while in nanoparticles it is very close to water (compare the main text and section 1.4 in supporting information). The resulting core-shell particle has a radius of 37 nm, which is smaller than the radius of gyration R_g of 55 nm obtained from Guinier analysis of SLS data (Table S3). Radius of gyration R_g is defined as a root man square distance from the center of mass and that Guinier-analysis provide a radius of a sphere. This differences in analyses could be one of the reasons for deviation of both radii. Further possible causes for for the deviation between the values of the radius obtained from SANS and SLS: lower scattering contrast of the shell in SANS compared to SLS, different q-range during the measurement, slight polydispersity of the sample and higher sensitivity of light scattering to bigger particles.[7] Cryogenic scanning electron Microscopy (cryoSEM) demonstrated that the size distribution of nanocapsules is monomodal. The approximate radius from cryoSEM is 46±13 nm (37 particles measured) and thus between the size from SANS and SLS. CryoSEM, thus, indicate that also a poor contrast of the shell in SANS could lead to this deviation between SANS and SLS. Note however, that exact size determination from cryoSEM is not possible as no sufficient number of particles can be measured to obtain a reliable size distribution and the exact positions of the edges of the particles cannot be always clearly determined. Moreover, cryoSEM might be affected by ice artefacts.

PFCE-loaded nanoparticles in D_2O and H_2O/D_2O 36/64 (*v:v*) mixture (match of PFCE) could be fitted using a model for fractal core-shell aggregates[8,9], using a simultaneous fitting approach to reduce the number of fitted parameters (Table S5).

In this model the form factor *P(q)* of the primary building block, which is a core-shell sphere, is combined with a fractal structure factor *S(q*) described by Teixeira, as described in the main text already.[8] Thus, the absolute scattering intensity *I(q)* can be described as:

$$I(q) = P(q) \cdot S(q) + background$$

The scattering length density of the core and shell were left free, as it is known from NMR that water is present within polymeric network and is close to PFCE. Both SLDs of PFCE-core and PLGA-shell are increasing due to hydration with the solvent. For nanoparticles in H_2O/D_2O 61/39 (*v:v*) mixture, which was matching the PLGA, the fractal core-shell model did not provide physically realistic values for the shell, as it consist of PLGA, which was matched. However, this sample could be fitted using a model for fractal aggregates with spherical building blocks, which consist of PFCE. Furthermore, here the SLD of the spherical building block, is between SLD of pure PFCE and H_2O/D_2O-mixture indicating the hydration of PFCE.

Radius of gyration R_g of the nanoparticle can be calculated from the fractal core-shell model with[1]:

$$R_g = \sqrt{D_f \cdot (D_f + 1) \cdot \xi^2/2}$$

with D_f the fractal dimension and ξ the correlation length.

The resulting R_g = 98 nm and thus smaller than R_g of 130 nm from SLS. However, there two values of R_g have a different definition. Guinier-analysis provides R_g of a sphere, whereas the R_g from SANS model corresponds to R_g of fractal system. Further deviations between both methods could be, again, caused by polydispersity of nanoparticles, or by lower scattering contrast of the shell compared to PFCE core, or the different q-range used in SANS and SLS. For calculation of size form SLS we used q-values between 6.8×10^{-4} Å^{-1} and 1.3×10^{-3} Å^{-1}, to meet the requirement for Guinier analysis $q\times R\leq 1$, while SANS was measured at $q>1.4\times10^{-3}$ Å^{-1} and could therefore underestimate the radius of gyration. Finally, the approximate radius from cryoSEM was 100±20 nm (39 particles measured) and thus very close to R_g from SANS. However, despite the fact that this is again a different "type" of radius, also in case of this sample it was difficult to accurately measure the particles. Thus, the cryoSEM is providing an indication of size rather than the exact size of the particles.

1.3 Solid State NMR

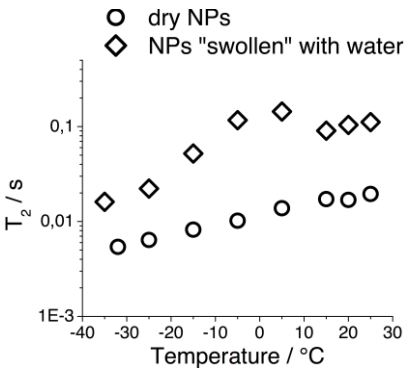

Figure S7. T_2 of dry nanoparticles, and nanoparticles incubated with water measured at solid state NMR at different temperatures**.**

1.4 Heteronuclear Overhauser Enhancement Spectroscopy (HOESY)

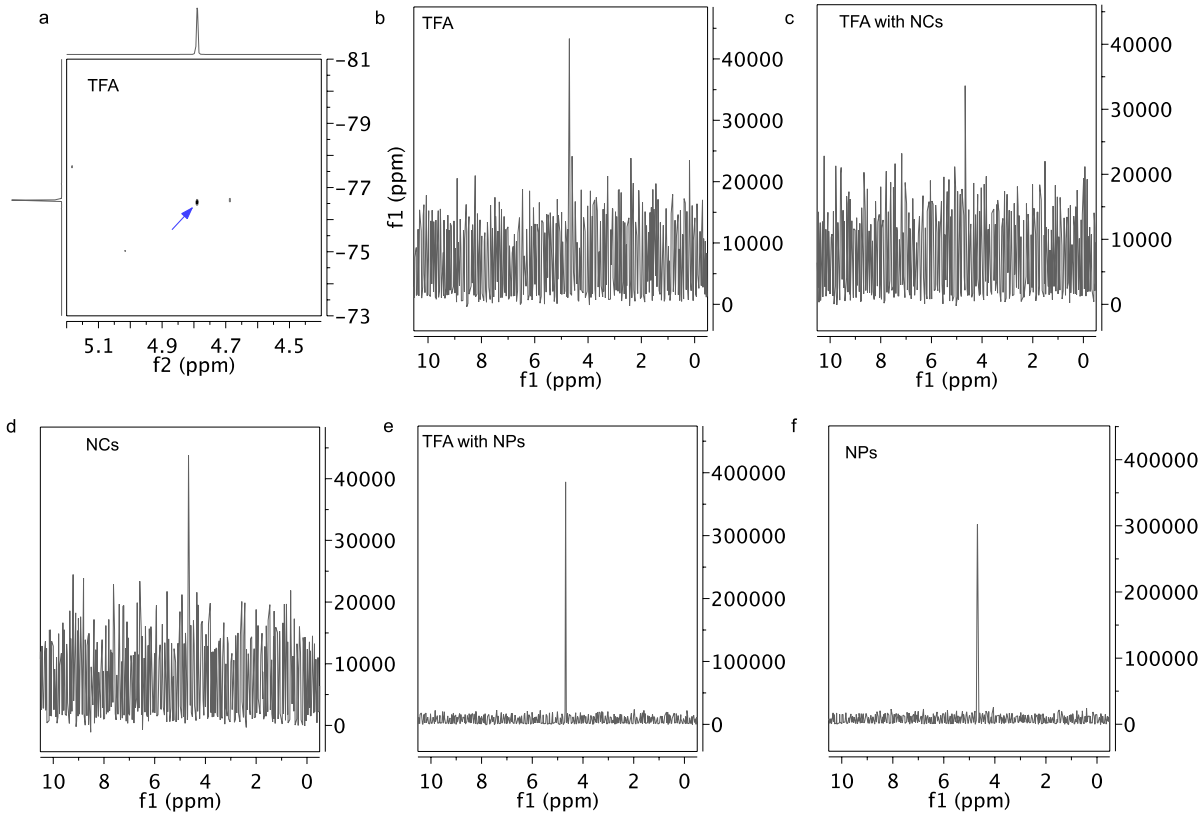

Figure S8. 1H detected 1H-19F HOESY of nanoparticles and nanocapsules compared to TFA alone. All samples D2O. a) HOESY spectrum of TFA alone. b) internal projection of HOE of TFA alone. c) internal projection of HOE of TFA which was added to nanocapsules d) internal projection of HOE of PFCE from nanocapsules e) internal projection of HOE of TFA which was added to nanoparticles f) internal projection of HOE of PFCE from nanoparticles. While signal-to-noise ratio of nanocapsules and internal TFA are similar to TFA without particles, nanoparticles and TFA with nanoparticles display higher SNR, indicating that water and TFA are both inside the network of nanoparticles.

Table S8. SNR of nanoparticles and capsules with TFA as internal reference compared to external TFA reference.

Sample	SNR
TFA alone	6
TFA (ref. nanoparticles)	48
TFA (ref. nanocapsules)	4
PFCE in nanoparticles	40
PFCE in nanocapsules	5

Supplementary Discussion 2: Hydration of PFCE by HOESY measurements.

HOESY[10] is typically a non-quantitative technique. To be still able to compare the HOE signal between nanoparticles and nanocapsules we added TFA as an internal reference to both samples. Additionally, we performed HOESY of TFA alone without adding any particles to measure the signal from the solution-phase-only interaction. The amount of TFA and the measurement parameters were kept the same for all three samples. Supplementary Figure S7 shows HOESY spectrum and the internal projection of TFA, which was measured alone, without adding any particles (a,b), internal projections of PFCE-H_2O HOE signals of nanocapsules (d) and nanoparticles (f) compared to internal projections of TFA signal (c, e), which was used as internal reference in both particle samples. Corresponding HOE spectra of nanoparticles and nanocapsules are shown in Figure 2 of the main manuscript. HOE of nanoparticles and TFA, which was added to nanoparticles as an internal reference display almost ten times higher signal-to-noise ratio (SNR) compared to nanocapsules and internal TFA reference of nanocapsules (Supplementary Table S7). Moreover TFA, which was measured without any particles, also have a low SNR similar to capsules. HOE is induced by a dipole-dipole interaction between molecules and therefore to detect HOE two main conditions need to be met: molecules have to be close to each other and they have stay close to each other long enough for relaxation to occur. In TFA solution without nanoparticles TFA molecules are highly mobile, with briefly-lasting hydrogen bonds to water, resulting only in low SNR. Similar behaviour is observed for nanocapsules. When, however, nanoparticles are added to TFA, SNR of HOE signal increases, indicating that the mobility of TFA molecules decreased compared to TFA without nanoparticles and TFA now can form more static complexes with water molecules. This decrease of mobility is most likely the result of the diffusion of TFA molecules inside polymeric network of nanoparticles together with water. Moreover, nanoparticles also display strong HOE between PFCE and water confirming the presence of water in the nanoparticle network close to PFCE. As both effects are absent in capsules, HOESY indicates major structural differences between both types of PFCE-loaded colloids.

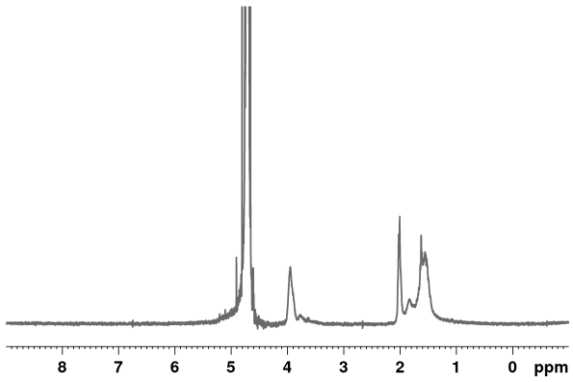

Figure S9. ^{1}H NMR spectrum of PFCE-PLGA nanoparticles shows typical PVA signals at 1-2 and 4 ppm. 400 MHz, D_2O.

2 Imaging of Nanoparticles

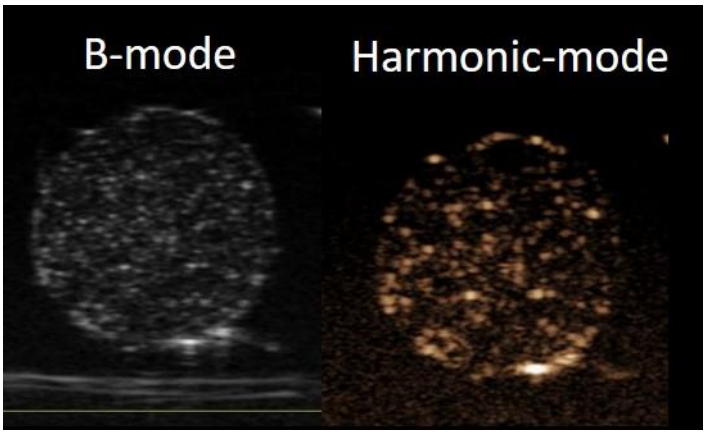

Figure S10. PFCE-capsules imaged in a gel phantom using B-mode and harmonic mode.

Video S1. The inguinal LN (INL) before injection of particles intranodally.

Video S2. The INL after injection of particles, showing a clear change in contrast.

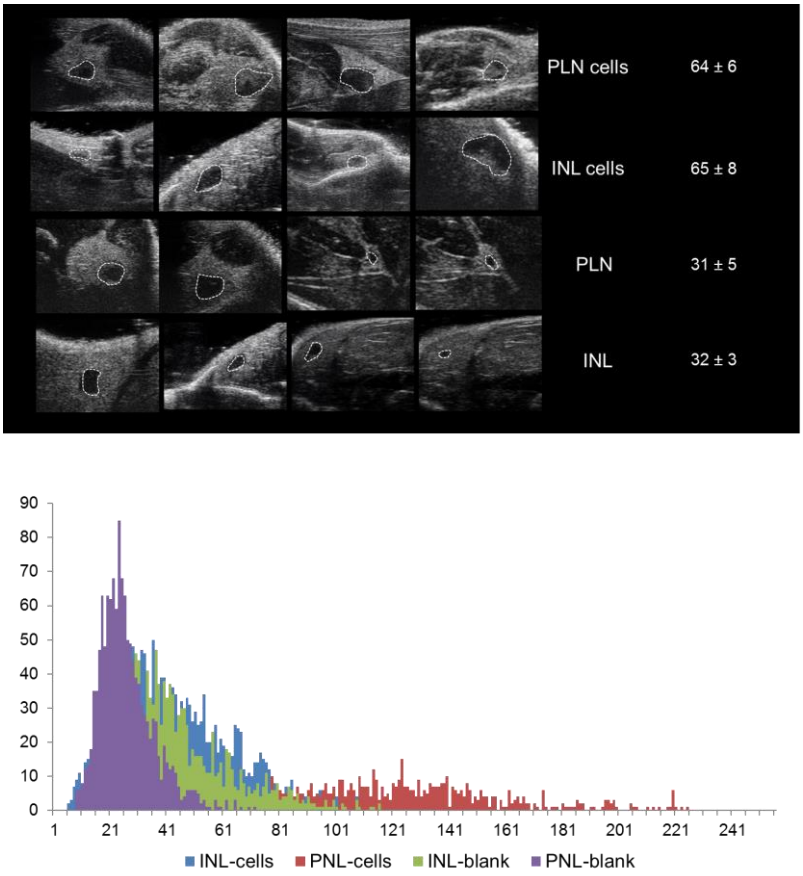

Figure S11. In vivo US images of the popliteal LN (PLN) and ILN are shown for mice that received either labelled cells (upper rows) or non-labelled cells (lower rows), along with the average pixel **i**ntensity over the node measured in ImageJ. The LNs are outlined in the images. A clear difference in pixel intensity was observed. This is also plotted in the lower panel.

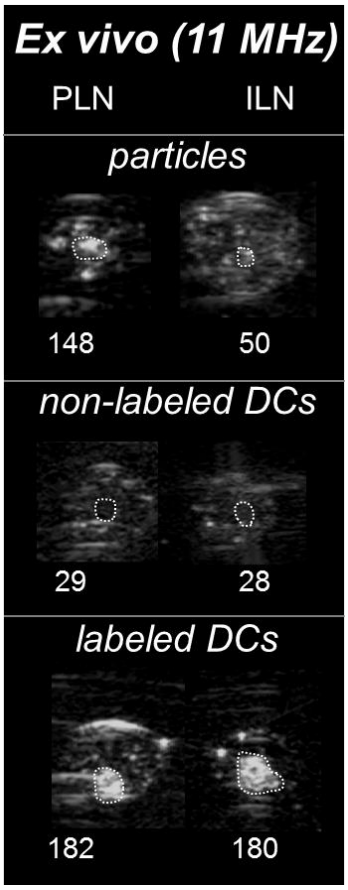

Figure S12. Ex vivo US images of excised lymph nodes (LNs) imaged in wells in a gel, using a clinical scanner at 11 MHz. This data indicates that the contrast is apparent even at clinical frequencies. Mean pixel intensity over the node is indicated as a guide for the eye.

References

1. Yang B, Lowe JP, Schweins R, Edler KJ. Small Angle Neutron Scattering Studies on the Internal Structure of Poly(lactide-co-glycolide)-block-poly(ethylene glycol) Nanoparticles as Drug Delivery Vehicles. *Biomacromolecules* **16** 457-464 (2015).
2. http://www.exfluor.com/msds.php?id=F15-crown-5
3. Lindner P, Schweins R. The D11 Small-Angle Scattering Instrument: A New Benchmark for SANS. *Neutron News* **21** 15-18 (2010).
4. Lindner P, Zemb T (eds). *Neutrons, X-rays and Light: Scattering Methods Applied to Soft Condensed Matter*. (Elsevier Science Ltd.: North Holland, 2002).
5. http://www.ill.eu/instruments-support/computing-for-science/cs-software/all-software/lamp/
6. Richard D, Ferrand M, Kearley GJ. Analysis and visualisation of neutron-scattering data. *Journal of Neutron Research* **4** 33-39 (1996).
7. Bantz C, Koshkina O, Lang T, Galla HJ, Kirkpatrick CJ, Stauber RH*, et al.* The surface properties of nanoparticles determine the agglomeration state and the size of the particles under physiological conditions. *Beilstein J. f Nanotechnol.* **5** 1774-1786 (2014).

8. Teixeira J. Small-angle scattering by fractal systems. *J Appl Crystallogr* **21** 781-785 (1988).
9. ftp://ftp.ncnr.nist.gov/pub/sans/kline/Download/SANS_Model_Docs_v4.10.pdf
10. Battiste J, Newmark RA. Applications of 19F multidimensional NMR. *Prog Nucl Magn Reson Spectrosc* **48** 1-23 (2006).